Robotica (2019) volume 37, pp. 779–800. © Cambridge University Press 2018
doi:10.1017/S0263574718001327

FAT-Based Robust Adaptive Control of Electrically Driven Robots in Interaction with Environment

Alireza Izadbakhsh†*, Payam Kheirkhahan† and Saeed Khorashadizadeh‡

† *Department of Electrical Engineering, Garmsar Branch, Islamic Azad University, Garmsar, Iran*
E-mail: kheirkhahan_payam@hotmail.com
‡ *Faculty of Electrical and Computer Engineering, University of Birjand, 615/97175 Birjand, Iran*
E-mail: s.khorashadizadeh@birjand.ac.ir

(Accepted November 19, 2018. First published online: December 18, 2018)

SUMMARY
This paper presents a robust adaptive impedance controller for robot manipulators using function approximation techniques (FAT). Recently, FAT-based robust impedance controllers have been presented using Fourier series expansion for uncertainty estimation. In fact, sinusoidal functions can approximate nonlinear functions with arbitrary small approximation error based on the orthogonal functions theorem. The novelty of this paper in comparison with previous related works is that the number of required regressor matrices in this paper has been reduced. This superiority becomes more dominant when the manipulator degrees of freedom (DOFs) are increased. First, the desired signals for motor currents are calculated, and then the desired voltages are obtained. In the proposed approach, only a simple model of the actuator and manipulator dynamics is used in the controller design and all the rest dynamics are treated as external disturbance. The external disturbances can then be approximated by Fourier series expansion. The adaptation laws for Fourier series coefficients are derived from a Lyapunov-based stability analysis. Simulation results on a 2-DOF planar robot manipulator including the actuator dynamics indicate the efficiency of proposed method.

KEYWORDS: Impedance control; Robot manipulator; Function approximation technique; Robust adaptive control.

1. Introduction

We have witnessed widespread industrial applications of robotic systems in which the interaction between the manipulator and environment should be managed automatically, such as assembly, polishing, grinding, mechanical part mating, and also medical surgery. One of the recent and high technological examples in this field is the exoskeleton robot.[1] Simultaneous control of both motion and force is the main challenge in these applications.[2,3] Many control laws have been developed to address this problem. However, it seems that impedance control[4,5] and hybrid position/force control[6,7] are the most important strategies.[8–11] In hybrid position/force control, one controller is responsible for position tracking in the free space and another controller is designed with the aim of force control along the directions in which position is constrained.[12] However, in impedance control, regulation of the dynamic performance of the system by careful selection of impedance parameters is considered.

* Corresponding author. E-mail: izadbakhsh_alireza@hotmail.com

Since impedance control requires the dynamical model of the manipulator, development of adaptive control algorithms is recommended to compensate for uncertainties. Many dynamical parameters of the manipulator such as mass and inertia of the links and the positions of the mass centers can be calculated using powerful softwares. Nevertheless, there may exist small errors, and consequently, the calculated or measured quantities are just nominal values. As a result, if the structure of the system dynamics is known, then adaptive control is a suitable option to compensate for the parametric uncertainties such as the differences between the obtained nominal values and their unknown correct values.[13]

Various adaptive impedance controllers have been developed in the last decades.[14–16] In ref. [14], adaptive free motion control has been applied to constrained robots. A direct adaptive impedance control scheme without the knowledge of the structure or the parameters of the robot dynamics has been presented in ref. [15]. To eliminate the need for acceleration signals, another adaptive impedance controller has been also designed in ref. [16]. The considerable point is that most of these controllers require the regressor matrix, since they are based on the linear parameterization of the manipulator dynamic model. Moreover, they are unable to handle unstructured uncertainty and external disturbance adequately, which is a missing link in almost all the addressed approach.[17]

Recently, adaptive control strategies have been developed which are based on function approximation techniques (FAT).[18–23] The main idea is representing the system uncertainties using orthogonal basis functions such as the Fourier series expansion, Bessel functions, Legendre polynomials, and so on. Differential equation has also been utilized as universal approximator.[24–26] In these strategies, the regressor matrices are not required which consequently simplifies the controller design procedure. Moreover, acceleration signals are not needed in this strategy.[27] These signals are usually contaminated by noise and will degrade the controller performance.

It should be noted that considering actuator dynamics can improve the controller performance in applications that high speeds are required or the load torque has a wide range of variations.[28] However, many previous approaches on impedance control of robot manipulators have excluded actuator dynamics from their controller design.[29–31] In other words, their control laws compute the applied torques to the robot joints. In practical implementations, these controllers should be modified by converting the torque signals to motor voltage signals. Thus, some voltage-based impedance controllers for robot manipulators have been presented in the literature.[32,33] However, their stability analysis is not complete due to excluding the current dynamics from the Lyapunov function. The voltage-based controller presented in ref. [33] is a model-based controller and requires exact values of the motor parameters and motor current derivatives. To solve these problems, this paper presents a robust voltage-based impedance controller considering motor current dynamics.

In this paper, an FAT-based robust impedance controller is designed for electrically driven robot manipulators. The MIMO structure of electrically driven robot is firstly considered as a simple uncertain nonlinear system maintaining the coverage of interaction among joints and treating the coupling effect as uncertainty. The lumped uncertainty, including parameter uncertainties, and modeling error can then be approximated by Fourier series expansion. According to ref. [34], robot dynamics are described by some sinusoidal and constant terms. Thus, Fourier series is a more suitable candidate for approximation of these functions. The adaptation laws for the Fourier series coefficients will be obtained based on the stability analysis. The superiority of proposed method over standard FAT-based adaptive impedance controllers is simplicity and reducing the number of regressor matrices. Consider an n-degree of freedom (n-DOF) robot manipulator. Suppose that for approximation of the inertia matrix, centrifugal/Coriolis matrix, gravitational vector, and the external voltage vectors, β_D, β_C, β_g, and β_f terms of Fourier series as the basis functions have been utilized. As a result, the weighting matrices (the Fourier series coefficients) in the standard FAT-based adaptive impedance controllers are of the dimensions $n^2\beta_D \times n$, $n^2\beta_C \times n$, $n\beta_g \times n$, and, $n\beta_f \times n$, respectively.[28] If n is increased, it is obvious that these dimensions will become greater. However, the proposed approach in this paper requires two weighting matrices with dimensions of $n\beta_\Xi \times n$ and $n\beta_f \times n$, where β_Ξ and β_f denote the number of basis functions utilized for approximation of lumped uncertainties.

This paper is organized as follows: Following the introduction, in Section 2, a task space dynamic model of electrically driven robot interacting with environment is presented. Section 3 presents the standard FAT-based adaptive impedance control scheme. The proposed control strategy and stability analysis are given in Section 4. Section 5 illustrates the simulation results using a 2-DOF planar

https://doi.org/10.1017/S0263574718001327 Published online by Cambridge University Press

robot manipulator including the actuator dynamics and finally, conclusions are drawn in Section 6. In what follows, we use the notation $\lambda_{\min}(\bullet)$ and $\lambda_{\max}(\bullet)$ to indicate the minimum and maximum eigenvalues, respectively, of a positive-definite bounded matrix. The norm of vector $y \in \Re^n$ is defined as $\|y\| = \sqrt{y^T y}$ and that of matrix $\|A(y)\| = \sqrt{\lambda_{\max}(A(y)^T A(y))}$.

2. Dynamic Equation of Electrically Driven Robot

The mathematical dynamics model of a rigid-link electrically driven robot having n-DOf in contact with the environment is described by [35, 36]

$$D(q)\ddot{q} + C(q, \dot{q})\dot{q} + g(q) = HI - J^T(q)F_{ext} \tag{1}$$

$$L\dot{I} + RI + K_b\dot{q} = u(t) \tag{2}$$

where q, $\dot{q}$, and $\ddot{q}$ denote the $n \times 1$ vectors of generalized link position, velocity, and acceleration, respectively; $D(q) \in \Re^{n\times n}$ is a symmetric positive-definite matrix, $C(q, \dot{q})\dot{q} \in \Re^n$ is the vector of Coriolis/centrifugal forces, $g(q) \in \Re^n$ is the vector of gravitational forces, $H \in \Re^{n\times n}$ is an invertible constant diagonal matrix characterizing the electro-mechanical conversion between the current vector and the torque vector, $I \in \Re^n$ is the vector of motor armature currents, $J(q) \in \Re^{n\times n}$ is Jacobian matrix, and $F_{ext} \in \Re^n$ is external force exerted by the robot at the end-effector. The constant positive-definite diagonal matrices $L \in \Re^{n\times n}$, $R \in \Re^{n\times n}$, and $K_b \in \Re^{n\times n}$ represent the electrical inductance, the electrical resistance, and the back EMF effects, respectively, of the actuators. Also, $u(t) \in \Re^n$ denotes the control input voltage applied for the joint actuators.

When controlling the dynamic behavior of the end-effector/environment interactions comes to be a main concern, it is often desirable to describe the manipulator dynamics in its operational space. Let $h \in \Re^n$ be a task space vector defined by [37]

$$h = \phi(q) \tag{3}$$

where $\phi(\bullet) \in \Re^n \to \Re^n$ is generally a nonlinear transformation describing the relation between the joint space and the task space. We can relate the velocities and accelerations in the task space to those in the joint space by the following relations:

$$\dot{h} = J(q)\dot{q} \tag{4}$$

$$\ddot{h} = J(q)\ddot{q} + \dot{J}(q)\dot{q} \tag{5}$$

Now, substituting Eqs. (4) and (5) into Eq. (1), and multiplying both sides by $J(q)^{-T}$ yields

$$M(h)\ddot{h} + H(h, \dot{h})\dot{h} + G(h) = J(q)^{-T}HI - F_{ext} \tag{6}$$

where

$$\begin{aligned} M(h) &= J(q)^{-T}D(q)J(q)^{-1} \\ H(h, \dot{h}) &= J(q)^{-T}\left(C(q, \dot{q}) - D(q)J(q)^{-1}\dot{J}(q)\right)J(q)^{-1} \\ G(h) &= J(q)^{-T}g(q) \end{aligned}$$

3. Standard Impedance Control

Impedance control utilizes a single control law, which attempts to regulate both position and force by specifying a dynamic relationship between them. This relationship is chosen to be a second-order linear impedance because such systems are well understood and simple to control. A standard impedance control law is shown in Eq. (7), where M_t, B_t, and k_t are constant positive-definite matrices, representing the desired inertia, damping, and stiffness system matrices in task space. Vectors h and h_d represent the actual and the desired end-effector positions, and F_{ext} represents the generalized force the environment exerts upon the end-effector

$$M_t(\ddot{h} - \ddot{h}_d) + B_t(\dot{h} - \dot{h}_d) + k_t(h - h_d) = -F_{ext} \tag{7}$$

https://doi.org/10.1017/S0263574718001327 Published online by Cambridge University Press

The target impedance parameters are specified by the user and have the dimensions of the task space. They cause the manipulator to exhibit the dynamics of a multi-directional mass–spring–damper system. The target impedance matrices are typically chosen to be diagonal, resulting in uncoupled response along each principle direction of h. With this in mind, Huang and Chen [28] proposed the standard adaptive impedance controller using FAT and introduced the following target impedance:

$$M_t(\ddot{h}_t - \ddot{h}_d) + B_t(\dot{h}_t - \dot{h}_d) + k_t(h_t - h_d) = -F_{ext} \tag{8}$$

where $h_t \in \Re^n$ is the state vector of the reference model (8). The FAT-based controller is designed such that h converges to h_t asymptotically, which yields convergence of the new target impedance (8) to (7) as desired. It does not require any knowledge of the system dynamics' parameters, except for the Jacobian matrix and torque constant. However, as mentioned in Section 1, weighting matrices (Fourier series coefficients) with large dimensions impose a considerable computational load in its real-time implementation. In the next section, we present a simpler FAT-based adaptive impedance controller for rigid-link electrically driven robot interacting with the environment.

4. Control Design

Based on the aforementioned strategy, an FAT-based adaptive impedance controller is developed that eliminates elaboration and computational burden in standard FAT-based adaptive impedance control strategy[28] proposed for robotic systems. The controller will be designed in the following order. At first, fictitious control law I_d is designed for I, which is not actual control input of the manipulator. Next, the actual control signal $u(t)$ is constructed in (2) to ensure convergence of I to I_d which results in convergence of h to desired trajectory h_t.

4.1. The output-tracking control loop

As a preliminary to the control design, let us define the actuator current tracking error as $e_I = (I - I_d) \in \Re^n$. Therefore, the robot dynamics (6) can be rewritten as

$$\ddot{h} = J(q)^{-T} H e_I + J(q)^{-T} H I_d + \Xi(t) \tag{9}$$

where $\Xi(t) \in \Re^n$ represents the lumped uncertainty denoted by

$$\Xi(t) = \big(I_n - M(h)\big)\ddot{h} - H(h, \dot{h})\dot{h} - G(h) - F_{ext} \tag{10}$$

and I_n denotes the identity matrix. Before we proceed with the details of controller derivation, consider the two following assumptions:

A1. The manipulator is operating away from any singularity.
A2. The nonlinear term $\Xi(t)$ is assumed to be an unknown function, and its variation bound is also assumed to be unavailable.

As a result of A2, traditional adaptive control scheme is not applicable. Under these circumstances, a Proportional-Derivative (PD) type control law supported by an auxiliary control input $\upsilon(t) \in \Re^n$ is proposed as

$$I_d(t) = H^{-1} J(q)^T \left(-K_p h - K_d \dot{h} + K_p \upsilon(t)\right) \tag{11}$$

where $K_p \in \Re^{n \times n}$ and $K_d \in \Re^{n \times n}$ are positive proportional and derivative gain matrices, respectively. Substituting (11) into (9) leads to

$$\dot{x}(t) = Ax(t) + B\big(J(q)^{-T} H e_I + K_p \upsilon(t) + \Xi(t)\big) \tag{12}$$

where

$$A = \begin{bmatrix} 0_n & I_n \\ -K_p & -K_d \end{bmatrix} \in \Re^{2n \times 2n}, \quad B = \begin{bmatrix} 0_n \\ I_n \end{bmatrix} \in \Re^{2n \times n}, \quad x(t) = \begin{bmatrix} h^T & \dot{h}^T \end{bmatrix}^T \in \Re^{2n}$$

Now, we develop an algorithm to adjust the control input $\upsilon(t)$. To that end, we introduce a reference model as

$$\dot{x}_d(t) = Ax_d(t) + BK_p \upsilon_d(t) \tag{13}$$

https://doi.org/10.1017/S0263574718001327 Published online by Cambridge University Press

where $\upsilon_d(t)$ represents the output of target impedance (8). It must be noted that the proposed approach is in fact a position-based impedance control scheme. Subtracting (13) from (12), we obtain

$$\dot{\tilde{x}}(t) = A\tilde{x}(t) + B\left(J(q)^{-T}He_I + K_p\aleph(t) + \Xi(t)\right) \tag{14}$$

where

$$\tilde{x}(t) = x(t) - x_d(t)\ ,\ \aleph(t) = \upsilon(t) - \upsilon_d(t) \tag{15}$$

Now, the control problem can be stated as designing a corrective control input $\aleph(t)$ such that $\tilde{x}(t)$ converges to zero or at least it is bounded by a constant. With this in mind, the universal approximation theorem will be used to represent $\Xi(t)$ as linear combinations of basis functions as

$$\Xi(t) = W_\Xi^T Z_\Xi + \varepsilon_\Xi \tag{16}$$

where $W_\Xi \in \Re^{n\beta_\Xi \times n}$ is weighting vector, β_Ξ is the number of basis function used, $Z_\Xi \in \Re^{n\beta_\Xi}$ is the vector of basis functions, and $\varepsilon_\Xi \in \Re^n$ is the approximation error of $\Xi(t)$. This approximation opens the opportunity to design the outer control loop $\aleph(t)$ based on compensation of the perturbation present in the plant. Now, making use of the same set of basis functions, we propose

$$\aleph(t) = -K_p^{-1}\hat{W}_\Xi^T Z_\Xi \tag{17}$$

where $\hat{W}_\Xi \in \Re^{n\beta_\Xi \times n}$ is the estimation of W_Ξ. When $\aleph(t)$ is generated by (17), it should be translated into the controller input $\upsilon(t)$ as

$$\upsilon(t) = \aleph(t) + \upsilon_d(t) \tag{18}$$

Now, substituting (16) and (17) into (14), we obtain the output-tracking loop dynamics as

$$\dot{\tilde{x}}(t) = A\tilde{x}(t) + B\left(J(q)^{-T}He_I + \tilde{W}_\Xi^T Z_\Xi + \varepsilon_\Xi\right) \tag{19}$$

where $\tilde{W}_\Xi = W_\Xi - \hat{W}_\Xi$ is the Fourier series weights approximation error.

4.2. The current tracking control loop

Here, the control objective is to design a control input $u(t)$ to realize the perfect motor current vector in (11) with the aim of reducing the error signal e_I as small as possible. It returns to this fact that, a constant-bounded disturbance will not destroy the stability result under robust control I_d which is a result of uniform ultimate boundedness of the tracking error using the Lyapunov-based theory of guaranteed stability of uncertain systems.[38] With this in mind, we propose the following control input:

$$u(t) = \hat{f} - K_c e_I \tag{20}$$

where $\hat{f}$ is the estimate of $f = L\dot{I}_d + RI + K_b\dot{q}$ and $K_c \in \Re^{n\times n}$ is a constant diagonal matrix of desired error dynamics. The current tracking loop dynamics with the controller in (2) can then be represented in the form of

$$L\dot{e}_I + K_c e_I = \hat{f} - f \tag{21}$$

Following the same procedure as in previous section, let us apply the function approximation representation:

$$f = W_f^T Z_f + \varepsilon_f \tag{22}$$

where $W_f \in \Re^{n\beta_f \times n}$ is a weighting matrix, $Z_f \in \Re^{n\beta_f}$ is a vector of basis functions, and $\varepsilon_f \in \Re^n$ is the approximation error vector. Utilizing the same set of basis function, f can be estimated as

$$\hat{f} = \hat{W}_f^T Z_f \tag{23}$$

https://doi.org/10.1017/S0263574718001327 Published online by Cambridge University Press

Define the parameter error vector as $\tilde{W}_f = W_f - \hat{W}_f$. Now, Eqs. (21)–(23) can be represented by

$$L\dot{e}_I + K_c e_I = -\tilde{W}_f^T Z_f + \varepsilon_f \tag{24}$$

which is a stable linear time-invariant system driven by the parameter error as well as the approximation error.

4.3. Stability analysis

To carry out the stability analysis of the closed-loop system formed by the robot dynamic models (1) and (2), together with the controllers (11) and (20), the following Lyapunov-like function candidate is proposed:

$$V\left(\tilde{x}, e_I, \tilde{W}_\Xi, \tilde{W}_f\right) = \frac{1}{2}\left[\tilde{x}^T P\tilde{x} + e_I^T L e_I + Tr\left(\tilde{W}_\Xi^T \Gamma_\Xi \tilde{W}_\Xi\right) + Tr\left(\tilde{W}_f^T \Gamma_f \tilde{W}_f\right)\right] \tag{25}$$

Differentiating (25) with respect to time and using (19) and (24) yield in

$$\begin{aligned}\dot{V}\left(\tilde{x}, e_I, \tilde{W}_\Xi, \tilde{W}_f\right) = {} & \frac{1}{2}\tilde{x}^T(A^T P + PA)\tilde{x} - e_I^T K_c e_I + \tilde{x}^T PBJ(q)^{-T} He_I \\ & + \tilde{x}^T PB\varepsilon_\Xi + e_I^T \varepsilon_f + \tilde{x}^T PB\tilde{W}_\Xi^T Z_\Xi - e_I^T \tilde{W}_f^T Z_f \\ & - Tr\left(\tilde{W}_\Xi^T \Gamma_\Xi \dot{\hat{W}}_\Xi + \tilde{W}_f^T \Gamma_f \dot{\hat{W}}_f\right)\end{aligned} \tag{26}$$

where $\Gamma_\Xi \in \Re^{n\beta_\Xi \times n\beta_\Xi}$ and $\Gamma_f \in \Re^{n\beta_f \times n\beta_f}$ are all positive-definite matrices. Since A is Hurwitz, one can arbitrarily choose a positive-definite matrix Q and let $P \in \Re^{2n\times 2n}$ be the unique symmetric positive-definite matrix that satisfies the Lyapunov equation:

$$A^T P + PA = -Q \tag{27}$$

Thus, substituting (27) into (26) we have

$$\begin{aligned}\dot{V}\left(\tilde{x}, e_I, \tilde{W}_\Xi, \tilde{W}_f\right) = {} & -\frac{1}{2}\tilde{x}^T Q\tilde{x} - e_I^T K_c e_I + \tilde{x}^T PBJ(q)^{-T} He_I \\ & + \tilde{x}^T PB\varepsilon_\Xi + e_I^T \varepsilon_f - Tr\left(\tilde{W}_\Xi^T\left(\Gamma_\Xi \dot{\hat{W}}_\Xi - Z_\Xi \tilde{x}^T PB\right)\right) \\ & - Tr\left(\tilde{W}_\Xi^T\left(\Gamma_f \dot{\hat{W}}_f + Z_f e_I^T\right)\right)\end{aligned} \tag{28}$$

By selecting the updated laws as

$$\begin{aligned}\dot{\hat{W}}_\Xi &= \Gamma_\Xi^{-1}\left(Z_\Xi \tilde{x}^T PB - \sigma_\Xi \hat{W}_\Xi\right) \\ \dot{\hat{W}}_f &= -\Gamma_f^{-1}\left(Z_f e_I^T + \sigma_f \hat{W}_f\right)\end{aligned} \tag{29}$$

where $\sigma_{(\bullet)}$ are positive numbers, (28) is simplified to

$$\begin{aligned}\dot{V}\left(\tilde{x}, e_I, \tilde{W}_\Xi, \tilde{W}_f\right) = {} & -\begin{bmatrix}\tilde{x}^T & e_I^T\end{bmatrix}\Lambda\begin{bmatrix}\tilde{x} \\ e_I\end{bmatrix} + \begin{bmatrix}\tilde{x}^T & e_I^T\end{bmatrix}P'\begin{bmatrix}\varepsilon_\Xi \\ \varepsilon_f\end{bmatrix} \\ & + \sigma_\Xi Tr\left(\tilde{W}_\Xi^T \hat{W}_\Xi\right) + \sigma_f Tr\left(\tilde{W}_f^T \hat{W}_f\right)\end{aligned} \tag{30}$$

where

$$\Lambda = \begin{bmatrix}\frac{1}{2}Q & -\frac{1}{2}PBJ(q)^{-T}H \\ -\frac{1}{2}PBJ(q)^{-T}H & K_c\end{bmatrix}$$

is a positive-definite matrix by proposer selection of K_c and Q, and $P' = \begin{bmatrix}PB & 0_{2n\times n} \\ 0_n & I_n\end{bmatrix} \in \Re^{3n\times 2n}$.

https://doi.org/10.1017/S0263574718001327 Published online by Cambridge University Press

Result 1. Suppose a sufficient number of basis functions are used and the approximation error can be ignored, then it is not necessary to include the σ-modification terms in (29). Hence, (30) can be reduced to

$$\dot{V}\left(\tilde{x}, e_I, \tilde{W}_\Xi, \tilde{W}_f\right) \leq -\left[\tilde{x}^T \; e_I^T\right] \Lambda \begin{bmatrix} \tilde{x} \\ e_I \end{bmatrix} \leq 0 \tag{31}$$

and asymptotic convergence of $\tilde{x}$ and e_I can be concluded using the Barbalat's Lemma.

Result 2. Owing to the existence of ε_Ξ and ε_I in (30), it is very easy to prove the following inequalities hold:

$$\begin{aligned} -\left[\tilde{x}^T \quad e_I^T\right] \Lambda \begin{bmatrix} \tilde{x} \\ e_I \end{bmatrix} + \left[\tilde{x}^T \quad e_I^T\right] P' \begin{bmatrix} \varepsilon_\Xi \\ \varepsilon_f \end{bmatrix} \\ \leq -\frac{1}{2}\lambda_{\min}(\Lambda) \left\| \begin{bmatrix} \tilde{x} \\ e_I \end{bmatrix} \right\|^2 + \frac{\lambda_{\max}^2(P')}{2\lambda_{\min}(\Lambda)} \left\| \begin{bmatrix} \varepsilon_\Xi \\ \varepsilon_f \end{bmatrix} \right\|^2, \\ Tr\left(\tilde{W}_{(\bullet)}^T \hat{W}_{(\bullet)}\right) \leq \frac{1}{2} Tr\left(W_{(\bullet)}^T W_{(\bullet)}\right) - \frac{1}{2} Tr\left(\tilde{W}_{(\bullet)}^T \tilde{W}_{(\bullet)}\right) \end{aligned} \tag{32}$$

Together with this relationship

$$\begin{aligned} V\left(\tilde{x}, e_I, \tilde{W}_\Xi, \tilde{W}_f\right) \leq \frac{1}{2}\Bigg[\lambda_{\max}(\Phi) \left\| \begin{bmatrix} \tilde{x} \\ e_I \end{bmatrix} \right\|^2 + \lambda_{\max}(\Gamma_\Xi) Tr\left(\tilde{W}_\Xi^T \tilde{W}_\Xi\right) \\ + \lambda_{\max}\left(\Gamma_f\right) Tr\left(\tilde{W}_f^T \tilde{W}_f\right)\Bigg] \end{aligned} \tag{33}$$

where $\Phi = \begin{bmatrix} P & 0 \\ 0 & L \end{bmatrix}$, we may write (30) in the form of

$$\begin{aligned} \dot{V}\left(\tilde{x}, e_I, \tilde{W}_\Xi, \tilde{W}_f\right) \leq -\mu V + \frac{1}{2}\left(\mu\lambda_{\max}(\Phi) - \lambda_{\min}(\Lambda)\right) \left\| \begin{bmatrix} \tilde{x} \\ e_I \end{bmatrix} \right\|^2 \\ + \frac{1}{2}\left(\mu\lambda_{\max}(\Gamma_\Xi) - \sigma_\Xi\right) Tr\left(\tilde{W}_\Xi^T \tilde{W}_\Xi\right) \\ + \frac{1}{2}\left(\mu\lambda_{\max}(\Gamma_f) - \sigma_f\right) Tr\left(\tilde{W}_f^T \tilde{W}_f\right) \\ + \frac{1}{2}\left[\frac{\lambda_{\max}^2(P')}{\lambda_{\min}(\Lambda)} \left\| \begin{bmatrix} \varepsilon_\Xi \\ \varepsilon_f \end{bmatrix} \right\|^2 + \sigma_\Xi Tr\left(W_\Xi^T W_\Xi\right) + \sigma_f Tr\left(W_f^T W_f\right)\right] \end{aligned} \tag{34}$$

By selecting $\mu \leq \min\left\{\frac{\lambda_{\min}(\Lambda)}{\lambda_{\max}(\Phi)}, \frac{\sigma_\Xi}{\lambda_{\max}(\Gamma_\Xi)}, \frac{\sigma_f}{\lambda_{\max}(\Gamma_f)}\right\}$, then (34) can be further derived as

$$\begin{aligned} \dot{V}\left(\tilde{x}, e_I, \tilde{W}_\Xi, \tilde{W}_f\right) \leq -\mu V + \frac{1}{2}\Bigg[\frac{\lambda_{\max}^2(P')}{\lambda_{\min}(\Lambda)} \left\| \begin{bmatrix} \varepsilon_\Xi \\ \varepsilon_f \end{bmatrix} \right\|^2 + \sigma_\Xi Tr\left(W_\Xi^T W_\Xi\right) \\ + \sigma_f Tr\left(W_f^T W_f\right)\Bigg] \end{aligned} \tag{35}$$

This implies that $\dot{V} < 0$ whenever

$$V > \frac{\lambda_{\max}^2(P')}{2\mu\lambda_{\min}(\Lambda)} \sup_{t_0 < \tau < t} \left\| \begin{bmatrix} \varepsilon_\Xi(\tau) \\ \varepsilon_f(\tau) \end{bmatrix} \right\|^2 + \frac{1}{2\mu}\left[\sigma_\Xi Tr\left(W_\Xi^T W_\Xi\right) + \sigma_f Tr\left(W_f^T W_f\right)\right] \tag{36}$$

Hence, we have proved that $\left(\tilde{x}, e_I, \tilde{W}_\Xi, \tilde{W}_f\right)$ are uniformly ultimately bounded. ■

https://doi.org/10.1017/S0263574718001327 Published online by Cambridge University Press

Because $\tilde{x}$ is bounded, boundedness of $x(t) = \left[h^T \ \dot{h}^T\right]^T$ can be obtained whereas x_d is bounded. Since the Jacobian matrix is bounded, boundedness of $\dot{q} = J(q)^{-1}\dot{h}$ can also be obtained whereas $\dot{h}$ is bounded. In addition, $q = \int_0^t J^{-1}(q)\dot{h}\mathrm{d}t + q(0)$ is also bounded, for finite operational times. Therefore, the robotic system will be stabilized with uniformly ultimately bounded (UUB) performance under the proposed design.

4.4. Performance evaluation

The stability analysis presented in the previous section only demonstrates boundedness of $(\tilde{x}, e_I, \tilde{W}_\Xi, \tilde{W}_f)$, but in practical applications the transient performance is also of great importance. For further development, we may solve the differential inequality in (35) to calculate the upper bound for $V(t)$:

$$\begin{aligned} V(t) \le e^{-\mu(t-t_0)}V(t_0) + \frac{\lambda_{\max}^2(P')}{2\mu\lambda_{\min}(\Lambda)} \sup_{t_0<\tau<t} \left\| \begin{bmatrix} \varepsilon_\Xi(\tau) \\ \varepsilon_f(\tau) \end{bmatrix} \right\|^2 \\ + \frac{1}{2\mu}\left[\sigma_\Xi Tr\left(W_\Xi^T W_\Xi\right) + \sigma_f Tr\left(W_f^T W_f\right)\right] \end{aligned} \tag{37}$$

Consider the lower bound of $V(t)$ in (25) as

$$\begin{aligned} V\left(\tilde{x}, e_I, \tilde{W}_\Xi, \tilde{W}_f\right) \ge \frac{1}{2}\lambda_{\min}(\Phi) \left\| \begin{bmatrix} \tilde{x} \\ e_I \end{bmatrix} \right\|^2 + \frac{1}{2}\Big[\lambda_{\min}(\Gamma_\Xi) Tr\left(\tilde{W}_\Xi^T \tilde{W}_\Xi\right) \\ + \lambda_{\min}(\Gamma_f) Tr\left(\tilde{W}_f^T \tilde{W}_f\right)\Big] \end{aligned} \tag{38}$$

This implies that $\left\| \begin{bmatrix} \tilde{x} \\ e_I \end{bmatrix} \right\| \le \sqrt{\frac{2V\left(\tilde{x}, e_I, \tilde{W}_\Xi, \tilde{W}_f\right)}{\lambda_{\min}(\Phi)}}$. Together with (37), we may compute the bound as

$$\begin{aligned} \left\| \begin{bmatrix} \tilde{x} \\ e_I \end{bmatrix} \right\| \le \sqrt{\frac{2V(t_0)}{\lambda_{\min}(\Phi)}} e^{\frac{-\mu(t-t_0)}{2}} + \sqrt{\frac{\lambda_{\max}^2(P')}{\mu\lambda_{\min}(\Phi)\lambda_{\min}(\Lambda)}} \sup_{t_0<\tau<t} \left\| \begin{bmatrix} \varepsilon_\Xi(\tau) \\ \varepsilon_f(\tau) \end{bmatrix} \right\| \\ + \frac{1}{\sqrt{\mu\lambda_{\min}(\Phi)}}\left[\sigma_\Xi Tr\left(W_\Xi^T W_\Xi\right) + \sigma_f Tr\left(W_f^T W_f\right)\right]^{\frac{1}{2}} \end{aligned} \tag{39}$$

This proves that the time history of $\left\| \begin{bmatrix} \tilde{x} \\ e_I \end{bmatrix} \right\|$ is bounded by an exponential function plus some constants. This also implies that by adjusting controller parameters, we may improve output error convergence rate. As a consequence,

$$\begin{aligned} \lim_{t\to\infty} \left\| \begin{bmatrix} \tilde{x} \\ e_I \end{bmatrix} \right\| \le \sqrt{\frac{\lambda_{\max}^2(P')}{\mu\lambda_{\min}(\Phi)\lambda_{\min}(\Lambda)}} \sup_{t_0<\tau<t} \left\| \begin{bmatrix} \varepsilon_\Xi(\tau) \\ \varepsilon_f(\tau) \end{bmatrix} \right\| \\ + \frac{1}{\sqrt{\mu\lambda_{\min}(\Phi)}}\left[\sigma_\Xi Tr\left(W_\Xi^T W_\Xi\right) + \sigma_f Tr\left(W_f^T W_f\right)\right]^{\frac{1}{2}} \end{aligned} \tag{40}$$

Considering the Frobenius norm definition, $\left(\left\|\tilde{W}_{(\bullet)}\right\|_F^2 = Tr\left(\tilde{W}_{(\bullet)}^T \tilde{W}_{(\bullet)}\right)\right)$, one can also obtain the following bounds for the weighting vectors $\tilde{W}_\Xi$ and $\tilde{W}_f$, respectively:

https://doi.org/10.1017/S0263574718001327 Published online by Cambridge University Press

$$\lim_{t\to\infty}\left\|\tilde{W}_{\Xi}\right\|_F^2 \le \sqrt{\frac{\lambda_{\max}^2(P')}{\mu\lambda_{\min}(\Gamma_{\Xi})\lambda_{\min}(\Lambda)}}\sup_{t_0<\tau<t}\left\|\begin{bmatrix}\varepsilon_{\Xi}(\tau)\\ \varepsilon_f(\tau)\end{bmatrix}\right\| + \frac{1}{\sqrt{\mu\lambda_{\min}(\Gamma_{\Xi})}}\left[\sigma_{\Xi}Tr\left(W_{\Xi}^T W_{\Xi}\right)+\sigma_f Tr\left(W_f^T W_f\right)\right]^{\frac{1}{2}} \tag{41}$$

$$\lim_{t\to\infty}\left\|\tilde{W}_{f}\right\|_F^2 \le \sqrt{\frac{\lambda_{\max}^2(P')}{\mu\lambda_{\min}(\Gamma_{f})\lambda_{\min}(\Lambda)}}\sup_{t_0<\tau<t}\left\|\begin{bmatrix}\varepsilon_{\Xi}(\tau)\\ \varepsilon_f(\tau)\end{bmatrix}\right\| + \frac{1}{\sqrt{\mu\lambda_{\min}(\Gamma_{f})}}\left[\sigma_{\Xi}Tr\left(W_{\Xi}^T W_{\Xi}\right)+\sigma_f Tr\left(W_f^T W_f\right)\right]^{\frac{1}{2}} \tag{42}$$

The transient performance analysis is then completed. ■

5. Simulation Results

In this section, we present simulation results for the proposed control scheme. The simulation task is carried out based on a 2-DOF planar robot including the actuator dynamics. The dynamic model of the robot system can be described in the form of Eq. (1) as[39]

$$\begin{aligned}
D(q) &= \begin{bmatrix} d_{11} & d_{12}\\ d_{21} & d_{22}\end{bmatrix}\\
d_{11} &= m_1 l_{c1}^2 + I_1 + m_2\left(l_1^2 + l_{c2}^2 + 2l_1 l_{c2}\cos(q_2)\right) + I_2\\
d_{21} &= d_{12} = m_2 l_{c2}^2 + m_2 l_1 l_{c2}\cos(q_2) + I_2\\
d_{22} &= m_2 l_{c2}^2 + I_2\\
C(q,\dot{q})\dot{q} &= \begin{bmatrix} -2m_2 l_1 l_{c2}\sin(q_2)\left(\dot{q}_1\dot{q}_2 + 0.5\dot{q}_2^2\right)\\ m_2 l_1 l_{c2}\sin(q_2)\dot{q}_1^2\end{bmatrix}\\
g(q) &= \begin{bmatrix} m_1 l_{c1} g\cos(q_1) + m_2 g\left(l_{c2}\cos(q_1+q_2) + l_1 g\cos(q_1)\right)\\ m_2 l_{c2} g\cos(q_1+q_2)\end{bmatrix}\\
J &= \begin{bmatrix} -l_1\sin(q_1) - l_2\sin(q_1+q_2) & -l_2\sin(q_1+q_2)\\ l_1\cos(q_1) + l_2\cos(q_1+q_2) & l_2\cos(q_1+q_2)\end{bmatrix}
\end{aligned} \tag{43}$$

where q_i $(i = 1, 2)$ is the joint angle, m_i is the mass of each link, l_i is the length of each link, and g is the gravity acceleration. The manipulator parameters are defined as $l_1 = l_2 = 0.75$ m, $l_{c1} = l_{c2} = 0.375$ m, $m_1 = m_2 = 0.5$ kg, and $I_1 = I_2 = 0.0234$ (kg.m^2). The actuator dynamic model parameters are selected as H = diag(10, 10) (N.m/A), R = diag(1, 1) Ω, L = diag(0.025, 0.025) H, and K_b= diag (1, 1) (V/rad/s).

The endpoint starts from $x(0)$=[0.8 m 0.75 m 0 0]^T to track a 0.2-m radius circle centered at (0.8 m,1 m) during 2 s. The initial condition of the target impedance states is the same as the initial value of the desired task space trajectory. We assume that the end-effector position can be obtained from a position sensor, such as vision systems, electromagnetic measurement systems, position sensitive detectors, or laser trackers. The values of the parameters in $M(h)$, $H(h, \dot{h})$, $G(h)$ are assumed to be unknown.

A vertical wall with a stiffness of $k_e = 5000$ (N/m)is located at $h_{x_e} = 0.95$ m along the y-axis. The environment dynamic was modeled as a regular spring, that is,

$$f_{ext} = k_e(h_x - h_{x_e}) \quad \text{for } h_x \ge h_{x_e} \tag{44}$$

https://doi.org/10.1017/S0263574718001327 Published online by Cambridge University Press

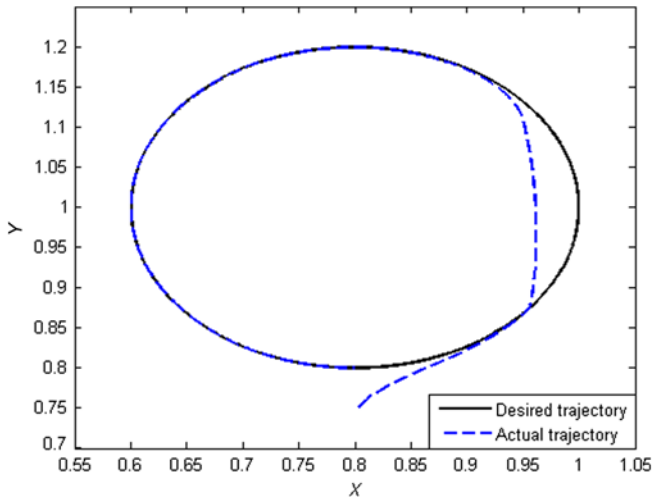

Fig. 1. Tracking performance of end-point in the task space (proposed approach).

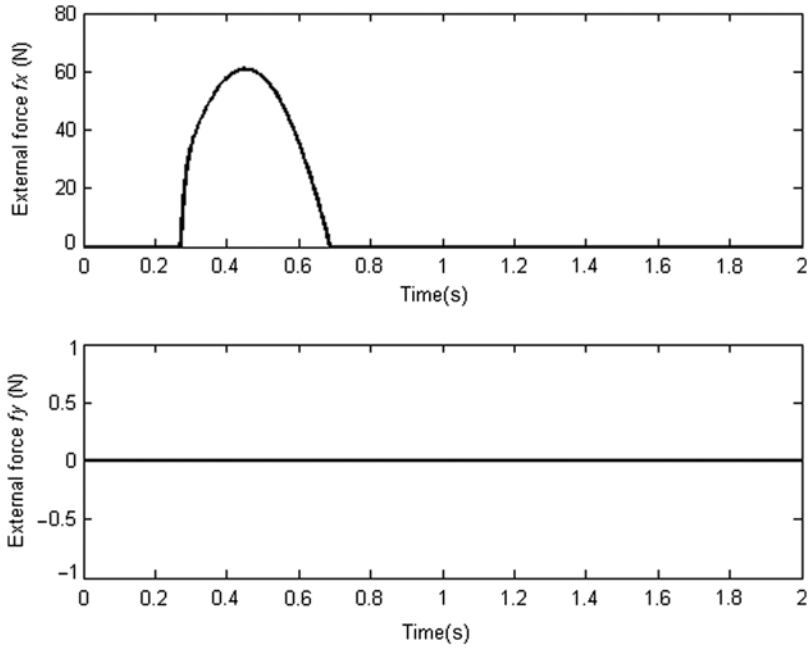

Fig. 2. External forces (proposed approach).

where f_{ext} is the force acting on the surface, k_e represents the environment dominant stiffness, h_x is the coordinate of the end-point in the X direction, and h_{x_e} denotes the location of the undeformed environment. Hence, the external force vector becomes $F_{ext} = \begin{bmatrix} f_{ext} & 0 \end{bmatrix}^T$. Parameter matrices in the target impedance are selected to be M_t = diag(0.5, 0.5), B_t = diag(100, 100), and k_t = diag(1500, 1500).[28] The controller parameters were selected as K_p = diag(1200, 1200), K_d = diag(70, 70), and K_c = diag(100, 100).

Let us select the 11-first terms of Fourier series expansion as the basis function for approximation of f and $\Xi(t)$. Therefore, $\hat{W}_f \in \Re^{22\times 2}$ and $\hat{W}_\Xi \in \Re^{22\times 2}$. The initial weighting vectors for the entries are also assigned to zero. The adaptive gain matrices are selected as $\Gamma_f = \Gamma_\Xi = 10^{-4} \times I_{22}$ where $I_{(\bullet)}$ is the identity matrix. In this step, we assume that the approximation error can be neglected, and

https://doi.org/10.1017/S0263574718001327 Published online by Cambridge University Press

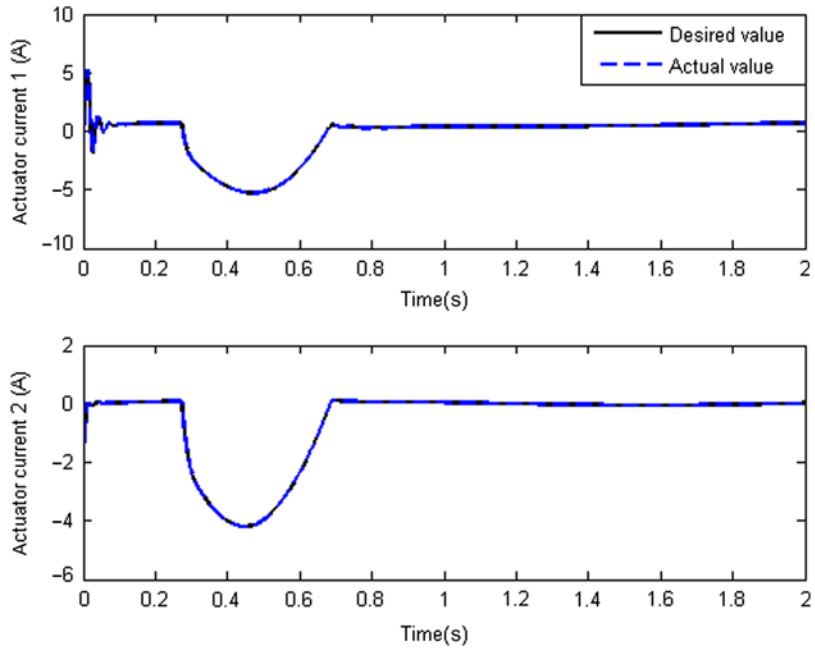

Fig. 3. Tracking in the current tracking loop (proposed approach).

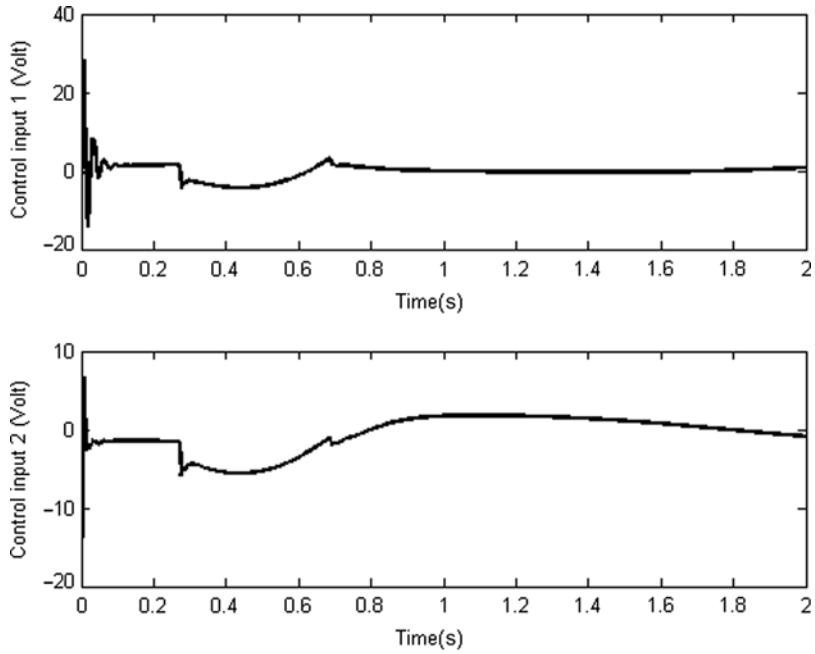

Fig. 4. Motor voltages (proposed approach).

hence the σ-modification parameters are chosen as $\sigma_f = \sigma_\Xi = 0$. In order to have quantitative results, the mean-squared-error (MSE) criterion has been selected.

Under these settings, Fig. 1 represents the desired and actual trajectories of the proposed adaptive impedance controller in the task space. The MSE for this figure is defined as $\text{MSE} = \frac{1}{2}\int_0^2 (e_x^2 + e_y^2)dt$ that takes the value of 0.001534.

Since the surface is away from the desired initial endpoint position, different phases of operation can be observed. The robot was initially moving in free space toward the wall. Following the

https://doi.org/10.1017/S0263574718001327 Published online by Cambridge University Press

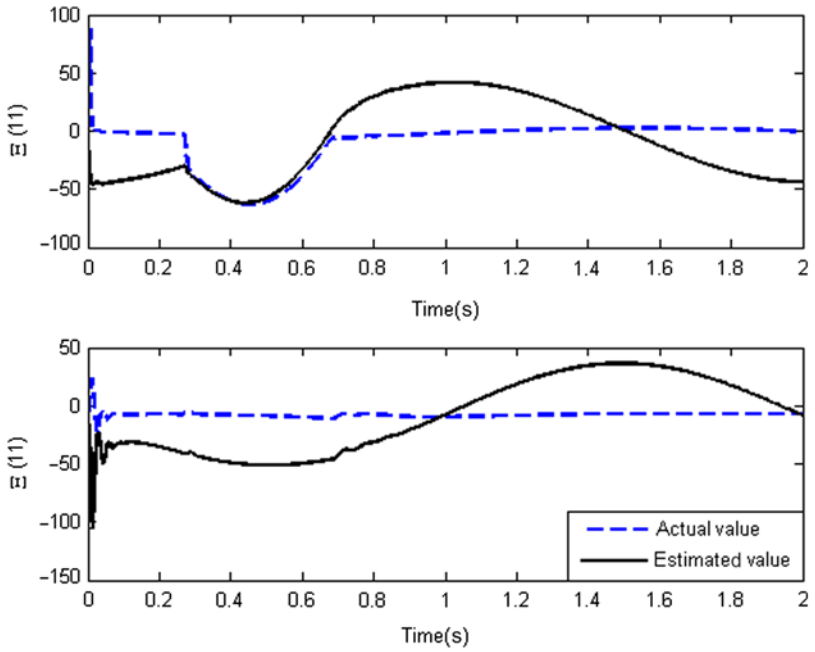

Fig. 5. Approximation of $\Xi(t)$ (proposed approach).

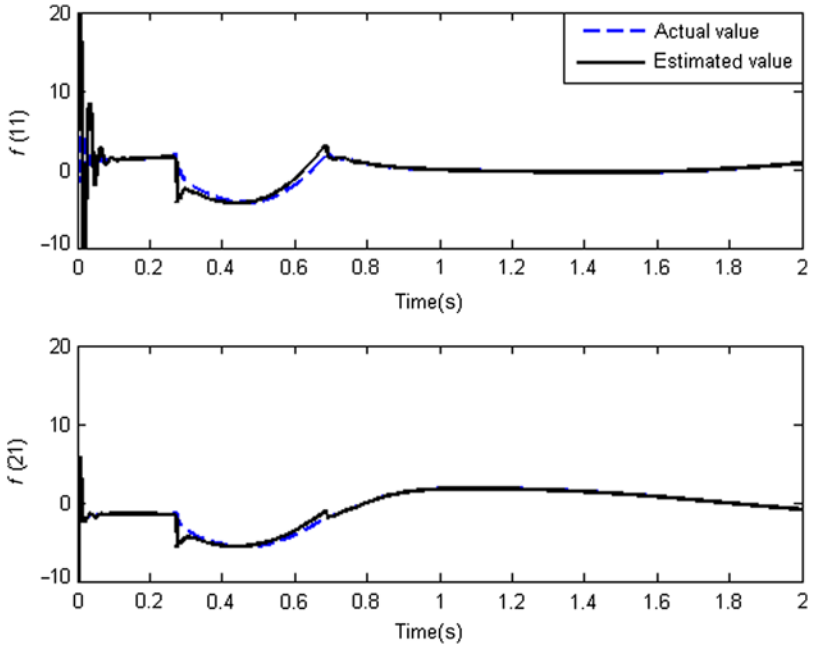

Fig. 6. Approximation of f (proposed approach).

commanded trajectory, the manipulator comes into contact with the wall at about $t = 0.271$ s (Fig. 2), enforcing the motion of the manipulator to stop in the normal direction to the wall. Because of the constraint from the wall and the tendency of the manipulator to follow the commanded trajectory, a collision force f_{ext}, shown in Fig. 2, is generated between the manipulator and the wall. The robot end-effector slides on the surface of the wall while exerting a certain normal force during this period.

https://doi.org/10.1017/S0263574718001327 Published online by Cambridge University Press

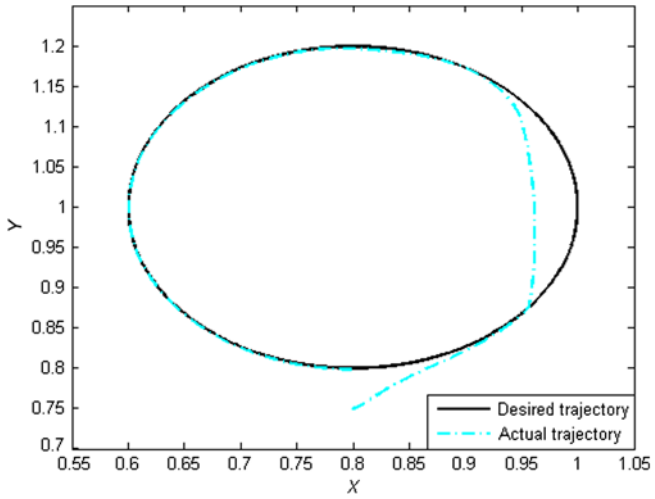

Fig. 7. Tracking performance of end-point in the task space (standard FAT-based impedance controller by Huang and Chen[28]).

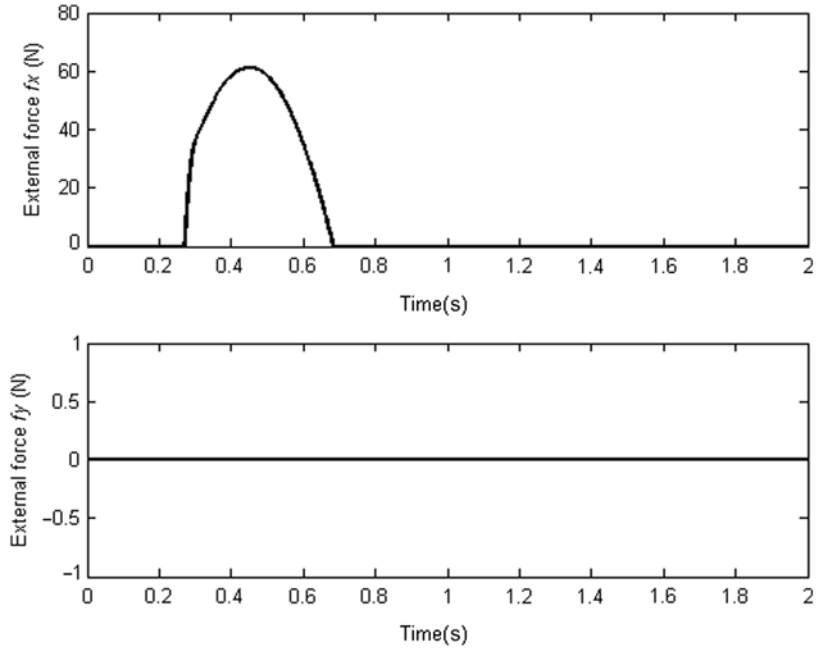

Fig. 8. External forces (standard FAT-based impedance controller by Huang and Chen[28]).

The performance in the current tracking loop is very good as shown in Fig. 3. The MSE for these signals is defined as MSE $= \frac{1}{2}\int_0^2 (e_{I1}^2 + e_{I2}^2)dt$ which shows the value of 0.001317. The control voltages to the actuators are reasonable that can be verified in Fig. 4. Finally, Figs. 5 and 6 represent the function approximation performance.

For completeness of the study and comparison purpose, the standard FAT-based adaptive impedance controller has been selected.[28] Details of the controller parameters are the same as those presented in ref. [28]. For this controller, Figs. 7–14 represent tracking performance, external force trajectories, tracking in the current loop, control efforts, and performance of the function approximation. The MSE for the tracking performance of this controller is about 0.003209 in Fig. 7. Also, the MSE criterion for the tracking in current loop of this controller in Fig. 9 is 0.0005312.

https://doi.org/10.1017/S0263574718001327 Published online by Cambridge University Press

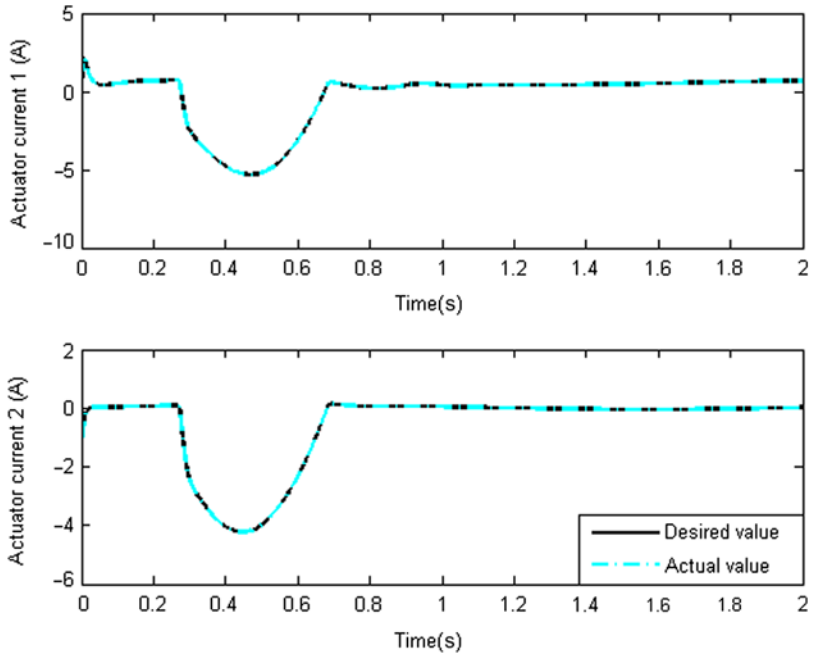

Fig. 9. Tracking in the current tracking loop (standard FAT-based impedance controller by Huang and Chen[28]).

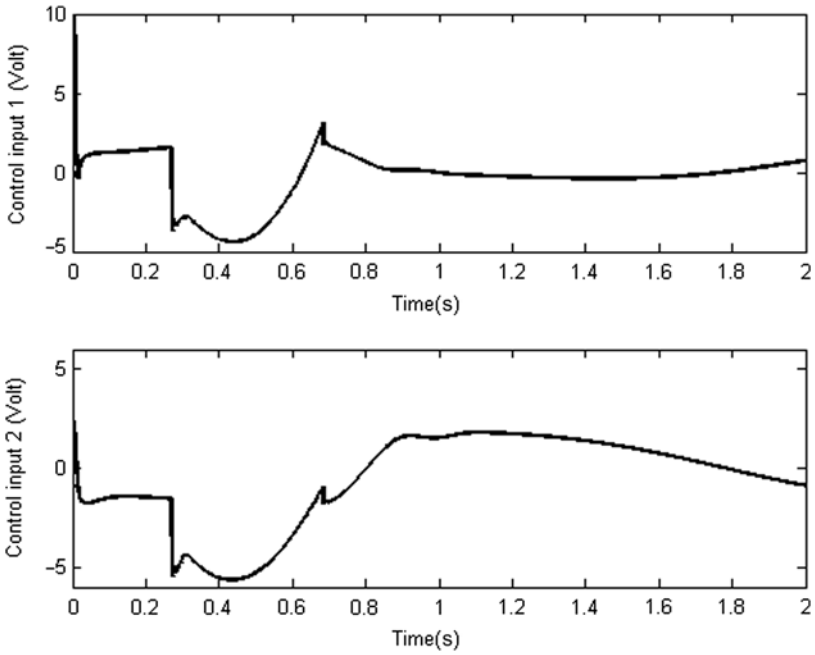

Fig. 10. Motor voltages (standard FAT-based impedance controller by Huang and Chen[28]).

As can be seen, both the proposed and standard FAT-based adaptive impedance controllers give the same results because of universal approximation property of Fourier series expansion. However, the new control scheme is much simpler and less computational than the standard form. In the standard adaptive impedance controllers, the weighting matrices dimensions for inertia matrix, centrifugal/Coriolis matrix, gravity vector, and the actuator disturbance voltage vectors (with the same number of sinusoidal functions ($\beta_D = \beta_C = \beta_G = \beta_f = 11$)) are $\hat{W}_D \in \Re^{44\times 2}$, $\hat{W}_C \in \Re^{44\times 2}$,

https://doi.org/10.1017/S0263574718001327 Published online by Cambridge University Press

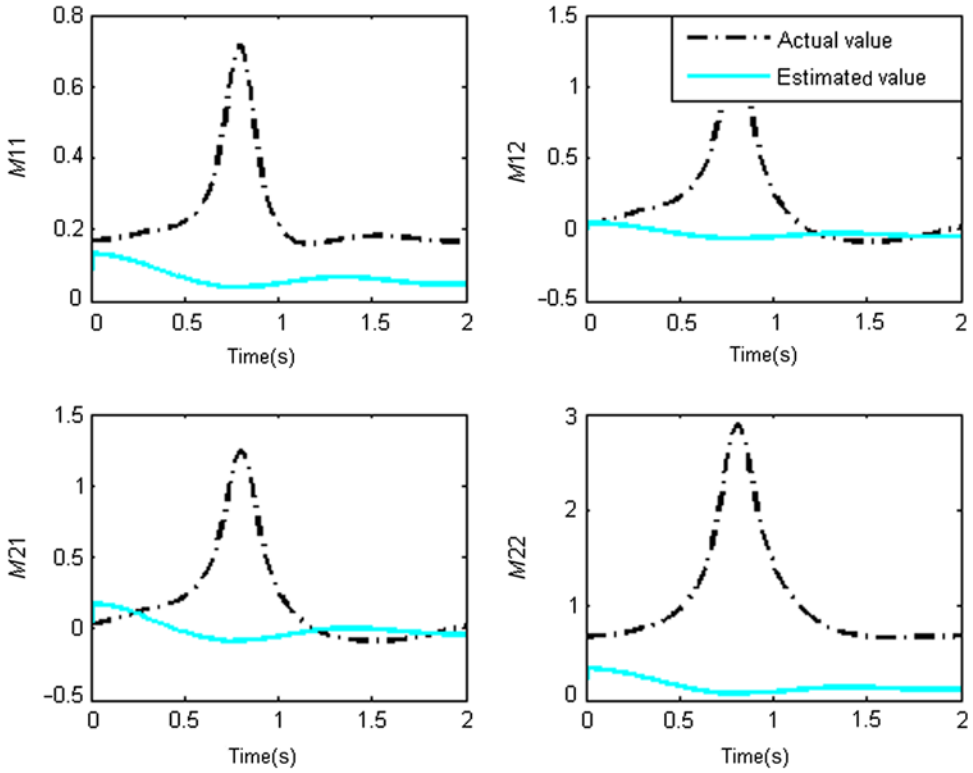

Fig. 11. Approximation of $M(h)$ (standard FAT-based impedance controller by Huang and Chen[28]).

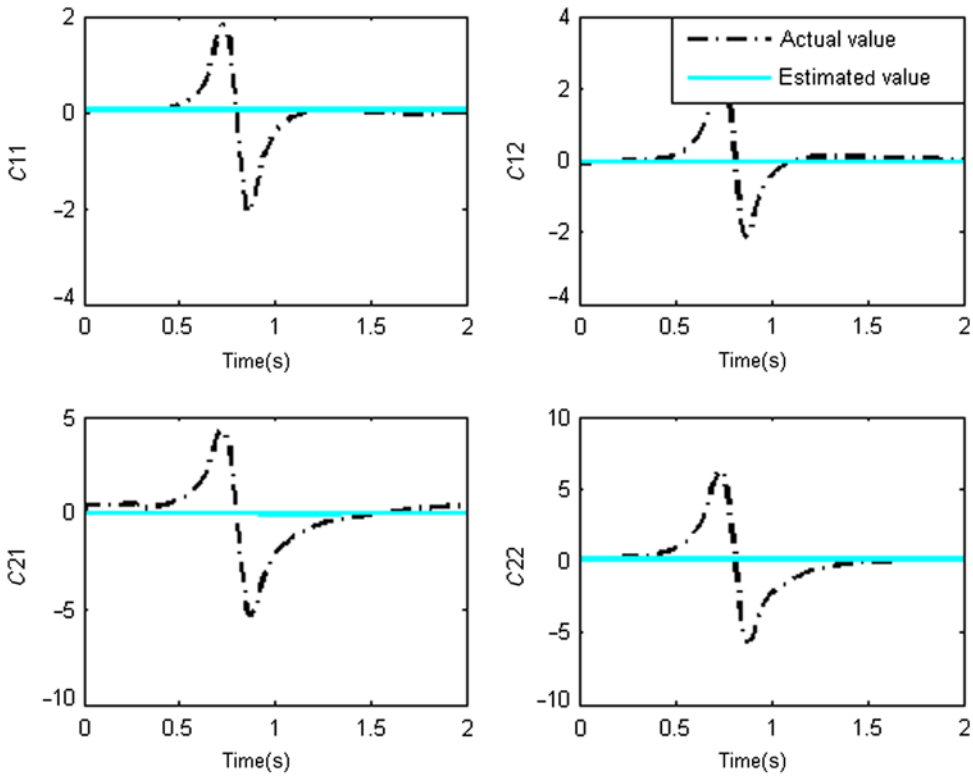

Fig. 12. Approximation of $C(h, \dot{h})$ (standard FAT-based impedance controller by Huang and Chen[28]).

https://doi.org/10.1017/S0263574718001327 Published online by Cambridge University Press

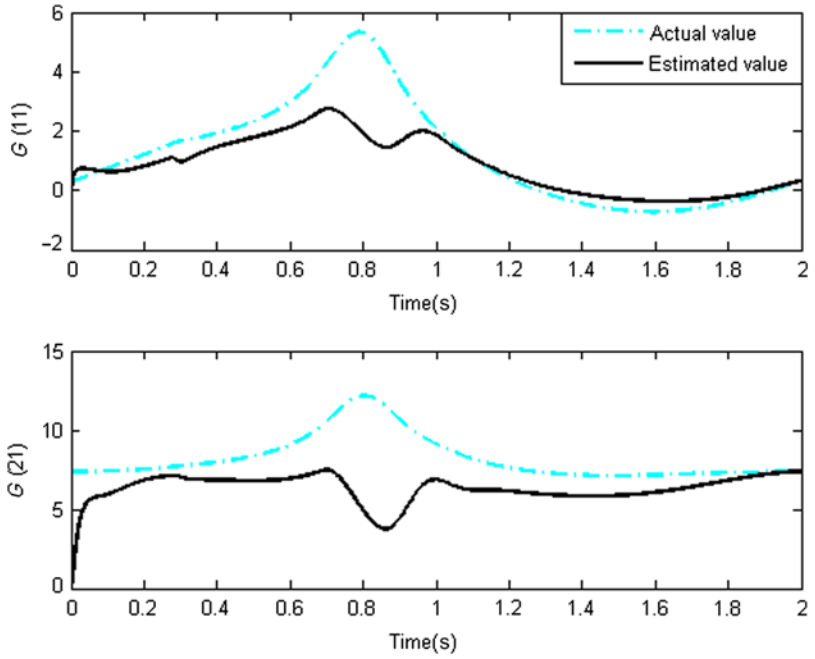

Fig. 13. Approximation of $G(h)$ (standard FAT-based impedance controller by Huang and Chen[28]).

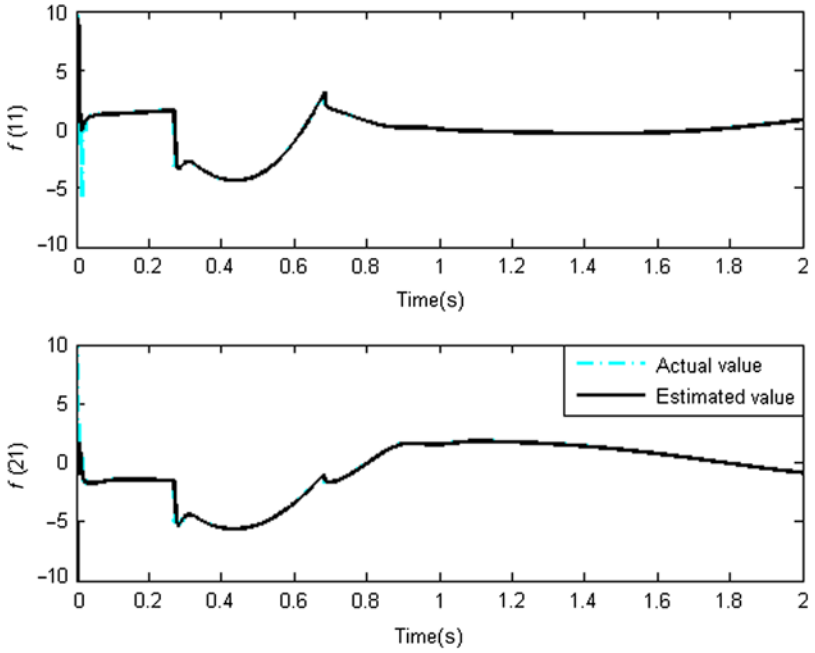

Fig. 14. Approximation of f (standard FAT-based impedance controller by Huang and Chen[28]).

$\hat{W}_g \in \Re^{22\times 2}$, and $\hat{W}_f \in \Re^{22\times 2}$, respectively, while the new control scheme requires two weighting matrices with dimension of $\hat{W}_\Xi \in \Re^{22\times 2}$ and $\hat{W}_f \in \Re^{22\times 2}$, under the same number of basis functions $\beta_\Xi = \beta_f = 11$.

For better illustration of the proposed algorithm superiority, variation of the payload, as the most important parameter that affects the controller performance, is considered. Toward this end, we

https://doi.org/10.1017/S0263574718001327 Published online by Cambridge University Press

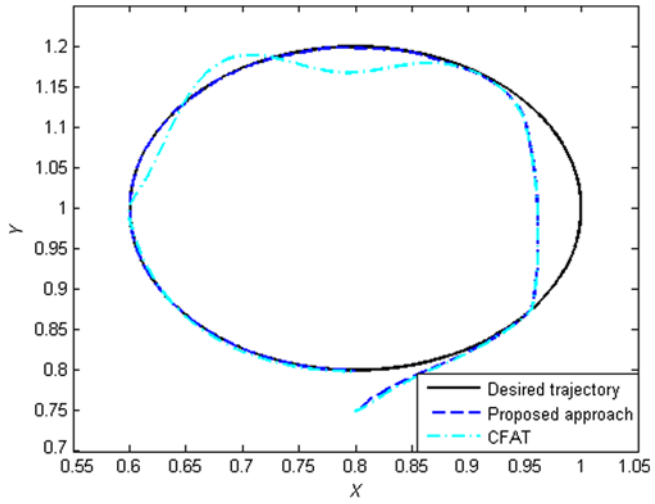

Fig. 15. Tracking performance under time varying payload.

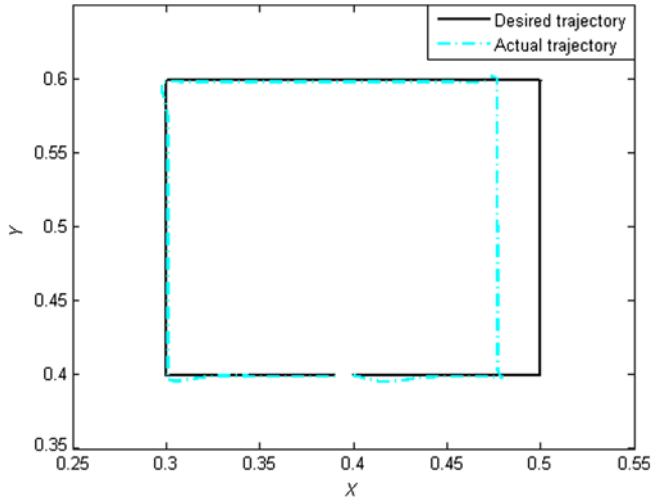

Fig. 16. Tracking performance of end-point in the task space (standard FAT-based impedance controller by Huang and Chen[28]).

assume that link 2 should pick up a heavy payload at $t = 0.8$ s and release it at $t = 1.5$ s during the tracking path. Since the load mass can be viewed as a part of the second link, the payload variation condition is that the mass of $\triangle m_2$ kg is added to the mass of link 2 at $t = 0.8$ s, that is, $m_2 + \triangle m_2$, and removed at $t = 1.5$ s. In this simulation, we take $\triangle m_2 = 4$ kg. The controller parameters are the same as before. Under these circumstances, Fig. 15 shows the tracking performances of the proposed approach and standard FAT-based adaptive impedance controller subject to the aforementioned variation.

The MSE for standard FAT-based adaptive impedance controller and the proposed approach are 0.01531 and 0.001855, respectively. From this simulation, it is concluded that the proposed control strategy can achieve a favorable performance and represents high robustness, while the standard FAT-based adaptive impedance algorithm does not give suitable tracking performance.

In order to study the performance of the proposed controller in tracking other command signals, a square trajectory in the X–Y plane has been considered. The controller parameters are the same as the circular trajectory. Assume that the aforementioned vertical wall is located at $h_{x_e} = 0.48$ m

https://doi.org/10.1017/S0263574718001327 Published online by Cambridge University Press

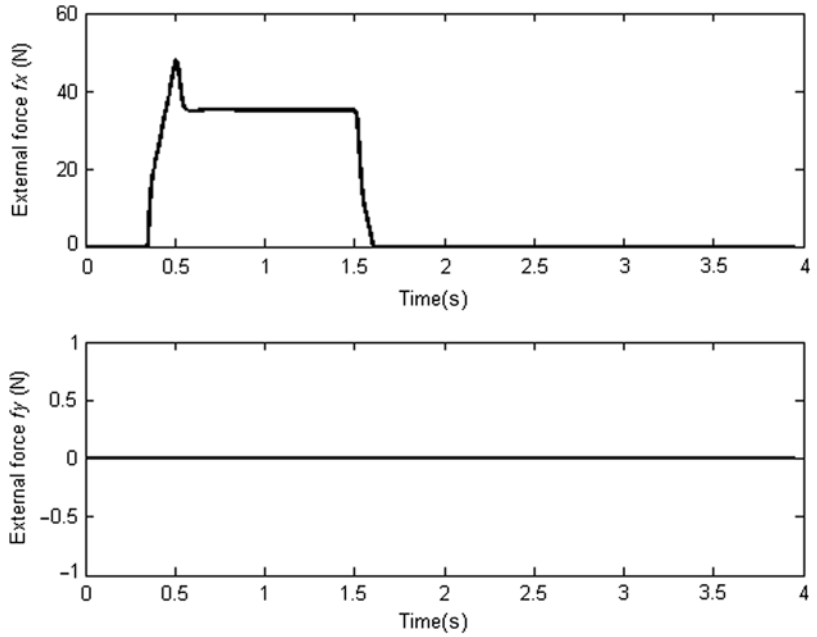

Fig. 17. External forces (standard FAT-based impedance controller by Huang and Chen[28]).

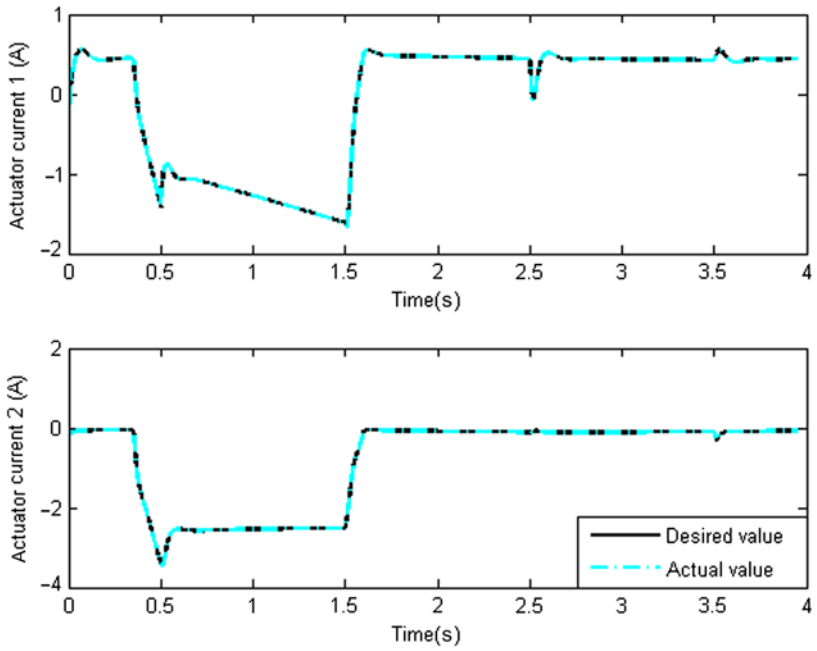

Fig. 18. Tracking in the current tracking loop (standard FAT-based impedance controller by Huang and Chen[28]).

along the Y-axis. The performance of standard FAT-based impedance controller in the X–Y plane is illustrated in Fig. 16. The MSE for this figure is 0.005455. The external forces for this controller are presented in Fig. 17. The tracking performance in the current control loop for this controller is given in Fig. 18. The MSE for this figure is 0.0005364. The control signals for this controller in tracking the square trajectory are plotted in Fig. 19. The tracking performance of the proposed controller in the X–Y plane for tracking this trajectory is presented in Fig. 20. The MSE for this figure is 0.001696.

https://doi.org/10.1017/S0263574718001327 Published online by Cambridge University Press

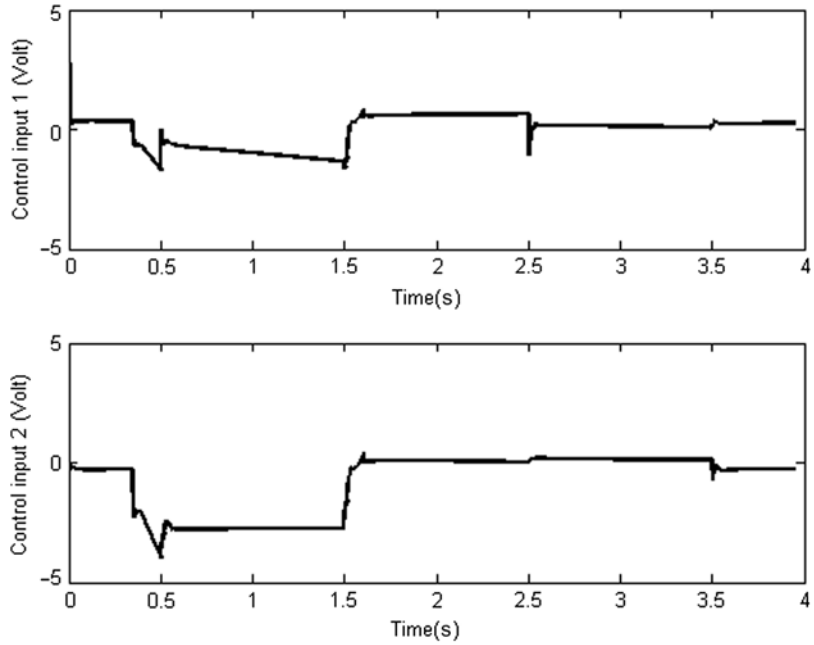

Fig. 19. Motor voltages (standard FAT-based impedance controller by Huang and Chen[28]).

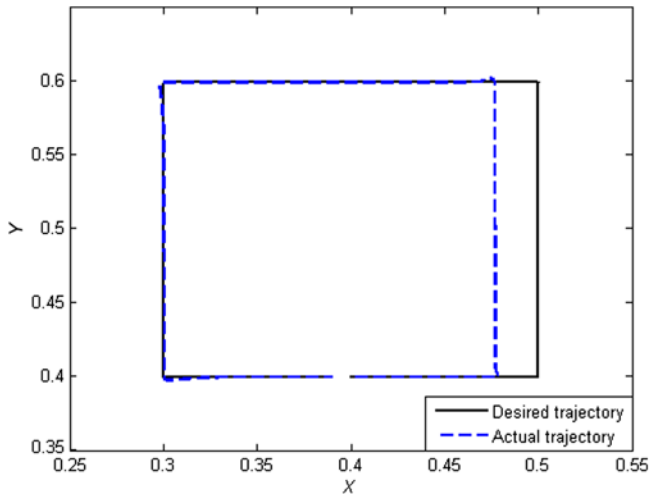

Fig. 20. Tracking performance of end-point in the task space (proposed approach).

The external forces for this controller are presented in Fig. 21. According to this figure, these signals are smooth and bounded. The tracking performance in the current control loop for this controller is given in Fig. 22. The MSE for these signals is 0.0005917. The control signals for the proposed controller in tracking the square trajectory are plotted in Fig. 23. As shown in this figure, motor voltages are bounded. Moreover, variation of payload for this trajectory has been simulated. It has been assumed that the aforementioned $\triangle m_2$ is added to the mass of link 2 at $t = 0.8$ s, that is, $m_2 + \triangle m_2$, and removed at $t = 2.5$ s. The tracking performances of both controllers in the X–Y plane are presented in Fig. 24. According to this figure, the proposed method is more robust and shows a more precise tracking. The MSE criterion for the standard FAT-based and the proposed approaches are 0.02476 and 0.003487, respectively.

https://doi.org/10.1017/S0263574718001327 Published online by Cambridge University Press

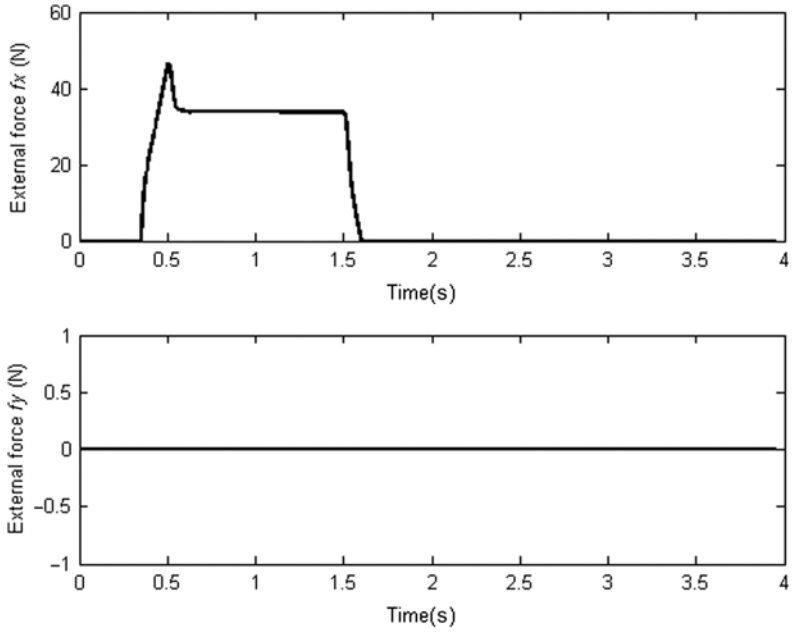

Fig. 21. External forces (proposed approach).

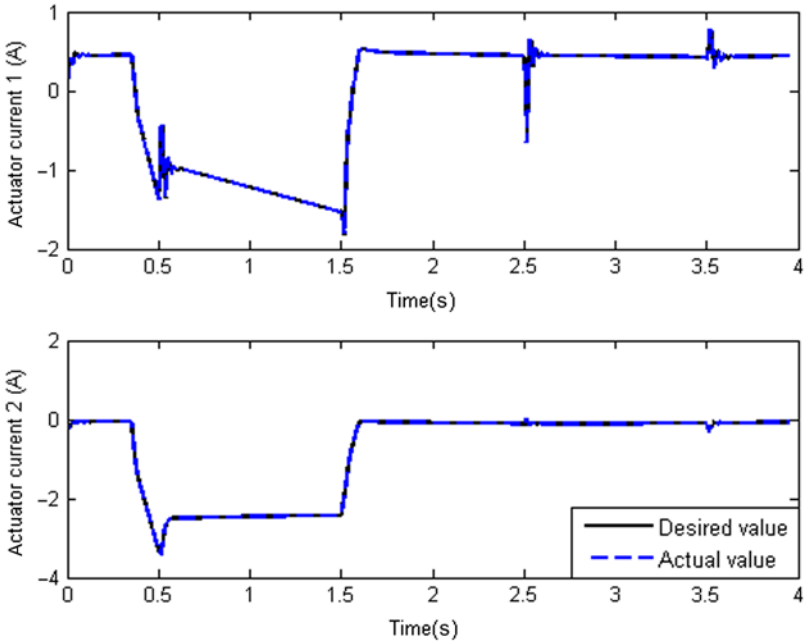

Fig. 22. Tracking in the current tracking loop (proposed approach).

6. Conclusion

An FAT-based robust impedance controller for electrically driven robots has been proposed in this paper. The control law considers the actuator dynamics and has been derived under the assumption that no information of the system and environment is in hand. The system stability has been verified by the Lyapunov's second method. The superiority of proposed method in comparison with standard FAT-based adaptive impedance controllers is reducing the number of regressor matrices. Simulation results on a 2-DOF planar robot manipulator actuated by DC motors verify the effectiveness of the proposed controller.

https://doi.org/10.1017/S0263574718001327 Published online by Cambridge University Press

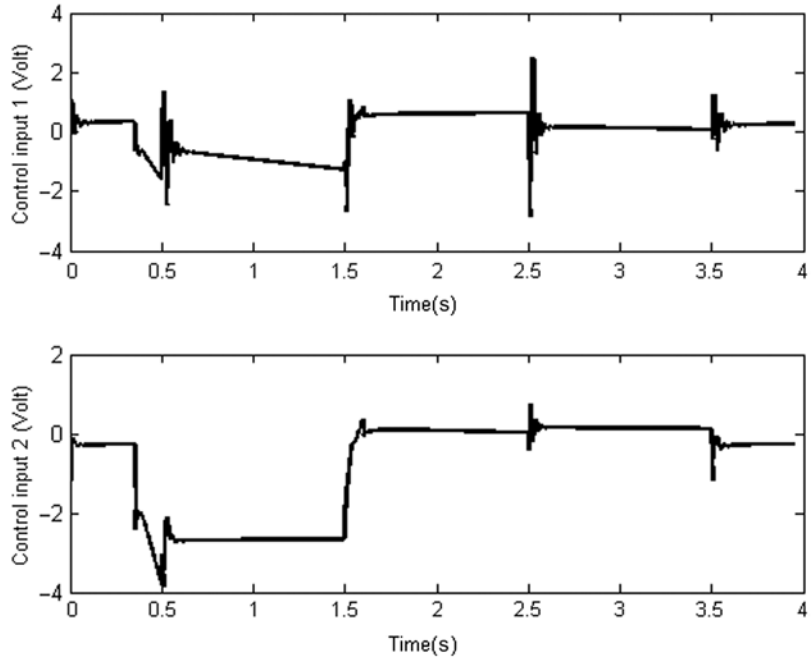

Fig. 23. Motor voltages (proposed approach).

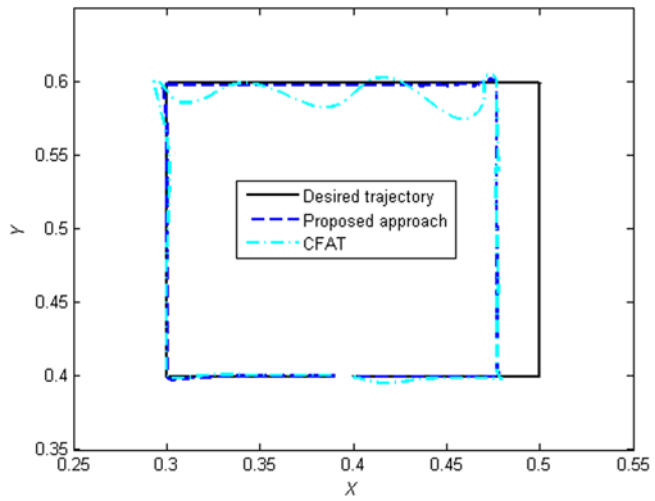

Fig. 24. Tracking performance under time varying payload on a square trajectory.

References

1. Y. Mao and S. K. Agrawal, "Design of a cable-driven arm exoskeleton (CAREX) for neural rehabilitation," *IEEE Trans. Robot.* **28**, 922–931 (2012).
2. M. W. Spong, F. L. Lewis and C. T. Abdallah, *Robot Control: Dynamics, Motion Planning, and Analysis* (IEEE Press, New York, 1993).
3. D. E. Whitney, "Historical perspective and state of the art in robot force control," *Int. J. Robot. Res.* **6**, 3–14 (1987).
4. N. Hogan, "Impedance control: An approach to manipulation: Part I-III," *ASME J. Dyn. Syst. Meas. Control* **107**, 1–24 (1985).
5. H. Kazerooni, "On the robot compliant motion control," *ASME J. Dyn. Syst. Meas. Control* **111**, 416–425 (1989).
6. M. Raibert and J. Craig, "Hybrid position/force control of manipulators," *ASME J. Dyn. Syst. Meas. Control* **102**, 126–133 (1981).
7. O. Khatib, "A unified approach for motion and force control of robot manipulators: The operational space formulation," *IEEE J. Robot. Autom.* **3**, 43–53 (1987).

https://doi.org/10.1017/S0263574718001327 Published online by Cambridge University Press

8. F. Almeida, A. Lopes and P. Abreu, "Force-impedance control: A new control strategy of robotic manipulators," *Recent Adv. Mechatr.* 126–137 (1999).
9. H. Kazerooni, P. Houpt and T. Sheridan, "Robust compliant motion for manipulators: Part II, design method," *IEEE J. Robot. Autom.* **2**, 93–105 (1986).
10. H. Seraji and R. Colbaugh, "Force tracking in impedance control," *Int. J. Robot. Res.* **16**, 97–117 (1997).
11. T. Boaventura, J. Buchli, C. Semini and D. G. Caldwell, "Model-based hydraulic impedance control for dynamic robots," *IEEE Trans. Robot.* **31**, 1324–1336 (2015).
12. V. F. Filaretov and A. V. Zuev, "Adaptive Force/Position Control of Robot Manipulators," *IEEE/ASME International Conference on Advanced Intelligent Mechatronics*, Xian, China (2008) pp. 96–101.
13. M. W. Spong, S. Hutchinson and M. Vidyasagar, *Robot Modelling and Control* (Wiley, Hoboken, 2006).
14. J. J. E. Slotine and W. Li, "Adaptive Strategies in Constrained Manipulation," *Proceedings of IEEE International Conference on Robotics and Automation*, Raleigh, NC, USA, **4** (1987) pp. 595–601.
15. R. Colbaugh, H. Seraji and K. Glass, "Direct Aadaptive Impedance Control of Manipulators." *Proceedings of IEEE Conference on Decision and Control*, Brighton, UK, **3** (1991) pp. 2410–2415.
16. R. R. Y. Zhen and A. A. Goldenberg, "An Adaptive Approach to Constrained Robot Motion Control," *Proceedings of IEEE International Conference on Robotics and Automation*, Nagoya, Japan, **2** (1995) pp. 1833–1838.
17. A. Izadbakhsh and M. M. Fateh, "Real-time robust adaptive control of robots subjected to actuator voltage constraint," *Nonlinear Dyn.* **78**, 1999–2014 (2014).
18. A. Izadbakhsh and M. Masoumi, "FAT-Based Robust Adaptive Control of Flexible-Joint Robots: Singular Perturbation Approach," *Annual IEEE Industrial Society's 18th International Conference on Industrial Technology (ICIT)*, Toronto, ON, Canada (2017) pp. 803–808.
19. A. Izadbakhsh, "Robust adaptive control of voltage saturated flexible joint robots with experimental evaluations," *AUT J. Model. Sim.* **50**(1), 31–38 (2018).
20. A. C. Huang, S. C. Wu and W. F. Ting, "A FAT-based adaptive controller for robot manipulators without regressor matrix: Theory and experiments," *Robotica* **24**, 205–210 (2006).
21. M. C. Chien and A. C. Huang, "Adaptive impedance controller design for flexible-joint electrically-driven robots without computation of the regressor matrix," *Robotica* **30**, 133–144 (2012).
22. A. Izadbakhsh, "FAT-based robust adaptive control of electrically driven robots without velocity measurements," *Nonlinear Dyn.* **89**, 289–304 (2017).
23. A. Izadbakhsh, "A note on the nonlinear control of electrical flexible-joint robots," *Nonlinear Dyn.* **89**, 2753–2767 (2017).
24. A. Izadbakhsh and S. M. R. Rafiei, "Robust Control Methodologies for Optical Micro Electro Mechanical Systems–New Approaches and Comparison," *Proceedings of the 13th International Power Electronics and Motion Control Conference (IEEE-EPE-PEMC)*, Poznan, Poland (2008) pp. 2102–2107.
25. A. Izadbakhsh and S. Khorashadizadeh, "Robust task-space control of robot manipulators using differential equations for uncertainty estimation," *Robotica* **35**(9), 1923–1938 (2017).
26. A. Izadbakhsh and S. Khorashadizadeh, "Robust impedance control of robot manipulators using differential equations as universal approximator," *Int. J. Control* **91**(10), 1–17 (2017).
27. M. C. Chien and A. C. Huang, "Adaptive impedance control of robot manipulators based on function approximation technique," *Robotica* **22**, 395–403 (2004).
28. A. C. Huang and M. C. Chien, *Adaptive Control of Robot Manipulators: A Unified Regressor-Free Approach*. (World Scientific Publishing Co. Pte. Ltd., Singapore, 2010).
29. R. Yang, C. Yang, M. Chen and J. Na "Adaptive impedance control of robot manipulators based on Q-learning and disturbance observer," *Syst. Sci. Control Eng.* **5**(1), 287–300 (2017).
30. F. Ficuciello, L. Villani and B. Siciliano, "Variable impedance control of redundant manipulators for intuitive human–robot physical interaction," *IEEE Trans. Rob.* **31**(4), 850–863 (2015).
31. J. Lee, P. H. Chang and R. S. Jamisola, "Relative impedance control for dual-arm robots performing asymmetric bimanual tasks," *IEEE Trans. Ind. Electr.* **61**(7), 3786–3796 (2014).
32. M. M. Fateh and V. Khoshdel, "Voltage-based adaptive impedance force control for a lower-limb rehabilitation robot," *Adv. Robot.* **29**(15), 961–971 (2015).
33. M. M. Fateh and R. Babaghasabha, "Impedance control of robots using voltage control strategy," *Nonlinear Dyn.* **74**(1–2), 277–286 (2013).
34. S. Khorashadizadeh and M. M. Fateh, "Uncertainty estimation in robust tracking control of robot manipulators using the Fourier series expansion," *Robotica* **35**(2), 310–336 (2017).
35. Z. Chu, J. Cui and F. Sun, "Fuzzy adaptive disturbance-observer-based robust tracking control of electrically driven free-floating space manipulator," *IEEE Syst. J.* **8**(2), 343–352 (2014).
36. D. M. Dawson, Z. Qu and J. J. Carroll, "Tracking control of rigid-link electrically-driven robot manipulators," *Int. J. Control* **56**(5), 991–1006 (1992).
37. H. Wang, W. Ren, C. C. Cheah and Y. Xie, "Dynamic Modularity Approach to Adaptive Inner/Outer Loop Control of Robotic Systems," *35th Chinese Control Conference*, Chengdu, China (IEEE, 2016) pp. 3249–3255.
38. A. Izadbakhsh and M. M. Fateh, "Robust Lyapunov-based control of flexible-joint robots using voltage control strategy," *Arab. J. Sci. Eng.* **39**, 3111–3121 (2014).
39. A. Izadbakhsh and S. M. R. Rafiei, "Endpoint perfect tracking control of robots– A robust non inversion-based approach," *Int. J. Control Autom. Syst.* **7**(6), 888–898 (2009).